RESEARCH ARTICLE

Key Points:
- Coherent radar data, Digisonde data, and modeling results are used to study the equatorial electrojet and sporadic E (E_s)
- The E region electric fields and E_s layers are analyzed during the November 2004 geomagnetic storm
- We show the variabilities of the zonal (E_y) and vertical (E_z) electric fields with storm time changes in the Brazilian equatorial E region

Correspondence to:
J. Moro,
juliano.moro@inpe.br;
julianopmoro@gmail.com

Equatorial *E* Region Electric Fields and Sporadic *E* Layer Responses to the Recovery Phase of the November 2004 Geomagnetic Storm

J. Moro[1,2] (iD), L. C. A. Resende[3], C. M. Denardini[3] (iD), J. Xu[1], I. S. Batista[3] (iD), V. F. Andrioli[1,3] (iD), A. J. Carrasco[4], P. P. Batista[3] (iD), and N. J. Schuch[2] (iD)

[1]State Key Laboratory of Space Weather, National Space Science Center, China Academy of Science, CAS, Beijing, China, [2]Southern Regional Space Research Center—CRS/COCRE/INPE, Santa Maria, Brazil, [3]National Institute for Space Research—INPE, São José dos Campos, Brazil, [4]Physics Department, Los Andes University, Mérida, Venezuela

Abstract Equatorial E region electric fields (EEFs) inferred from coherent radar data, sporadic-E (E_s) layers observed from a digital ionosonde data, and modeling results are used to study the responses of the equatorial E region over São Luís (SLZ, 2.3°S, 44.2°W, ~−7° dip angle), Brazil, during the super storm of November 2004. The EEF is presented in terms of the zonal (E_y) and vertical (E_z) components in order to analyze the corresponding characteristics of different types of E_s seen in ionograms and simulated with the E region ionospheric model. We bring out the variabilities of E_y and E_z components with storm time changes in the equatorial E region. In addition, some aspects of the electric fields and E_s behavior in three cases of weak, very weak, and strong Type II occurrences during the recovery phase of the geomagnetic storm are discussed. The connection between the enhanced occurrence and suppressions of the Type II irregularities and the q-type E_s (Es_q) controlled by electric fields, with the development or disruption of the blanketing sporadic E (Es_b) layers produced by wind shear mechanism, is also presented. The mutual presence of Es_q along with the Es_b occurrences is a clear indicator of the secular drift of the magnetic equator and hence that of the equatorial electrojet (EEJ) over SLZ. The results show evidence about the EEJ and E_s layer electrodynamics and coupling during geomagnetic disturbance time electric fields.

1. Introduction

The equatorial electrojet (EEJ) consists of a small Pedersen current driven by the zonal (E_y) electric field generated by tidal neutral winds and a large Hall current driven by the vertical (E_z) polarization electric field. The E_z component, in turn, is produced by an impeded Hall current driven by the primary E_y (Denardini et al., 2013; Forbes, 1981; Moro et al., 2016a, and references therein). The E_y component, eastward during the daytime, controls the vertical plasma transport in the low-latitude ionosphere and forms a critical input to models that predict ionospheric disturbances in real time (Maruyama et al., 2005; Scherliess et al., 2006). The E_z component drives the gradient drift instability, $E \times B$ (drifts with the electron flux that constitutes the EEJ), and produces the Type II irregularities that can act as scattering centers for HF and VHF radio waves (Devasia et al., 2004). Therefore, the accurate inference of the E_z component is essential in understanding the dynamical features of the EEJ for space weather monitoring, especially during geomagnetic disturbed periods, when Type II irregularities may be amplified or suppressed in a short time (Denardini et al., 2006).

The gradient drift instability mechanism is known to be responsible for the equatorial sporadic E layers (q-type E_s or Es_q) that occur inside the EEJ. These types of E_s are the diffuse and nonblanketing trace observed on daytime ionograms as a scattering of the radio signal that covers most of the frequency scale (Knecht & McDuffie, 1962). The Es_q is different from the E_s layer, since it is not an enhanced ionization of the plasma as the sporadic E layers of blanketing type (Es_b), produced by ionization convergence arising from the well-known wind shear theory, which ionization converges at the null points of vertical shears in meridional or zonal neutral wind components (Haldoupis, 2011; Hook, 1970; Lanchester et al., 1991; Whitehead, 1989). The basic distinction between both layer types is that the Es_q layer is always translucent to radio waves in ionograms, while the Es_b layers are highly dense and effectively block the access of the HF signal to the upper ionospheric layers (Piggot & Rawer, 1972; Resende et al., 2016; Resende, Denardini, & Batista, 2013).

The E_y and the E_z components of the E region electric fields (EEFs) in Brazil have been studied in terms of the Doppler shifts of Type II echoes detected with the 50 MHz backscatter coherent (RESCO) radar installed at São Luís (SLZ, 2.3°S, 44.2°W, ~−7° dip angle). Moro et al. (2016a) investigated the variability of the EEF components based on long-term RESCO soundings collected during the geomagnetic quiet days ($Kp \leq 3^+$) between 2001 and 2010 and compared the results with the electric field components inferred at the Jicamarca Radio Observatory (JRO, 11.9°S, 76.8°W, ~2° dip angle). The mean diurnal variations of E_y range from 0.21 to 0.35 mV/m between 8 and 18 h (LT) in the Brazilian sector, while the mean diurnal variations of the E_z range from 7.09 to 8.80 mV/m. However, the electric field components presented an interesting dependence with the dip equator secular displacement effect at SLZ (see Figure 1 in Moro et al., 2016a), which causes different variations in E_y and E_z at JRO. This result led to a study on the seasonal dependence of E_y and E_z by Moro et al. (2016b), which revealed for the first time the impact of the secular variation of the geomagnetic field on the EEJ in terms of electric fields.

The steady northwestward excursions of the geomagnetic field strongly influence the electrodynamics of the E region plasma over the eastern Brazilian region. The features of the EEF and, consequently, the EEJ and E_s are strongly affected and have been studied by many researches using data from radars, ionosondes, magnetometers, and computing modeling (Abdu et al., 1996; Abdu, Bittencourt, & Batista, 1981; Batista, Abdu, & Bittencourt, 1986; Batista et al., 2011; Denardini et al., 2013, 2015; Moro et al., 2016a, 2016b; Resende et al., 2016, 2017). The ionograms collected in SLZ show the presence of Es_q and Es_b layers. The mutual presence of Es_q layers produced by the electric fields and Es_b layers produced by wind shear is a clear indicator of the secular drift of the magnetic equator and hence that of the EEJ over eastern Brazil. Resende et al. (2016) studied the competition between tidal winds and electric fields in the formation of Es_b over SLZ. The authors reported an increase in the occurrence rates of Es_b since 2009, revealing that the EEJ has little or no influence there, confirming the results of Tsunoda (2008) about the anticorrelation characteristics between Es_b and the EEJ intensity and Moro et al. (2016b) about the secular variation of the geomagnetic field on the EEJ in terms of electric fields over SLZ.

The recent results about the inference of E_y and E_z at SLZ presented by Denardini et al. (2013, 2015) and Moro et al. (2016a, 2016b, 2016c) consider the electric fields inferred from RESCO data collected under quiet geomagnetic activity only. The study we report here is, however, restricted to the responses of the EEF observations at SLZ during the intense geomagnetic storm of November 2004. We focus in the study of the electrodynamic coupling between the auroral and EEJ plasma irregularities in eastern Brazil, which remains unclear during geomagnetic disturbed periods due to the dip equator secular displacement effect. We also bring out the variabilities of E_y and E_z during the storm time changes, not shown before for the E region at equatorial latitudes as far as we know. According to Resende et al. (2016) and Abdu et al. (2014), the Es_b layers are subject to the influence of E_z, and the theory about the connection between Es_b occurrence and E_z needs to be investigated with more details during geomagnetic storms, which we are also pursuing in this work. Therefore, the characteristics of the EEF and E_s observed at SLZ during the large and complex November 2004 geomagnetic storm are analyzed to evaluate the enhanced occurrence or suppressions of the EEJ plasma irregularities, that is, Type II irregularities. Finally, a connection with the formation or disruption of Es_q and Es_b layers is shown using Digisonde data and model in order to study this relationship over SLZ. The instrument locations used in this work and their relation to the magnetic equator are shown in Figure 1. The geomagnetic equator provided by the International Geomagnetic Reference Field model is shown as the red line for the year 2001 and the blue line for the year 2010.

2. Data Presentation and Modeling

Data from coherent backscatter and all-sky meteor radars, digital ionosonde, magnetometer, satellite, and model results are used to study the response of the equatorial E region to the intense geomagnetic storm of 10 November 2004. In the following, we briefly describe each set of data used in this work.

2.1. RESCO Coherent Backscatter Radar Data

The 50 MHz RESCO radar had been routinely used to measure the Doppler shifts of 3 m irregularities present in the EEJ between 8 and 18 local time (LT = UT − 3) from 1998 to 2009. The echoes received from 80 to 120 km of altitude are processed, providing in-phase and quadrature signals containing Doppler frequency
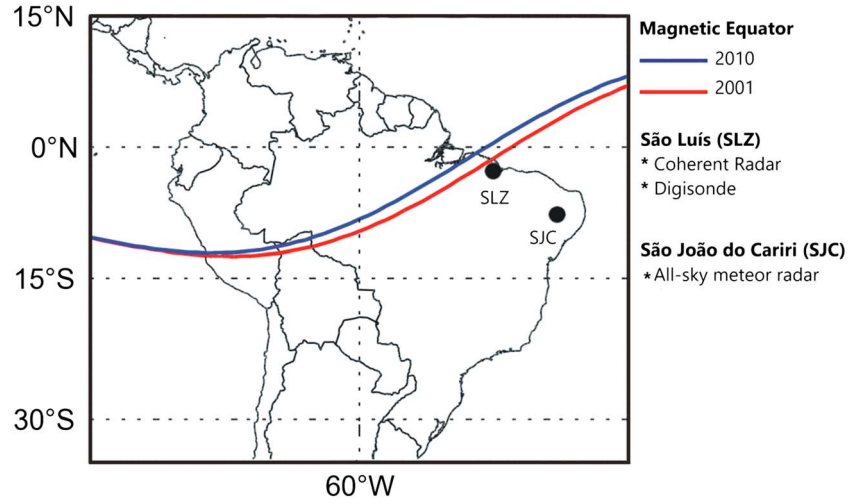
Figure 1. Measurements sites in Brazil used in this work and their relation to the magnetic equator.

and power information of the EEJ plasma irregularities. The RESCO height resolution is 2.6 km (3 km in range), and the time resolution is 2 min. Despite the 102.5, 105.1, 107.7, and 110.3 km ranges of RESCO radar heights being usually used to study the EEJ, in this work, we selected only the range from 103.9 to 106.5 km centered at 105.1 km because this range is located in the center of the EEJ.

A spectral decomposition technique is applied to every single spectrum to obtain the Doppler frequency of Type II echoes (f_{DII}, observed whenever the density gradient has a positive projection along E_z). The frequency f_{DII} is converted into Doppler velocities of Type II irregularities (V_{DII}) taking into account the RESCO operating frequency ($f_R = 50$ MHz) and the speed of light ($c \approx 3 \times 10^8 m/s$), as shown in equation (1):

$$V_{DII} = \frac{c}{2f_R} f_{DII},$$ (1)

where $c/2f_R = 3$ m. The resulted V_{DII} are grouped according to the height and time of data acquisition, aiming to obtain mean velocities at a given height and local time in order to have the horizontal component of these mean velocities along the radar beam. The drift velocity of E region electrons (V_e) in the EEJ is related with V_{DII} accordingly (equation (2)):

$$V_{DII} = \frac{V_e}{1 + \Psi_0} + \frac{V_i \Psi_0}{1 + \Psi_0},$$ (2)

where V_i is the ion velocity, $\Psi_0 = v_{in} v_{en}/\Omega_i \Omega_e$ is known as anisotropic factor and v_{in} and v_{en} are the ion-neutral and electron-neutral collision frequencies, respectively. The electron and ion gyrofrequencies are Ω_e and Ω_i, respectively. The ion motion, V_i (essentially due to neutral wind), can be neglected while deriving V_e from the observed Doppler velocity above 100 km (Devasia et al., 2004). Therefore, we neglected in this work the last term in equation (2) in order to derive the E_z component at 105.1 km by equation (3) (Cohen, 1973; Denardini et al., 2013; Moro et al., 2016a):

$$V_e = \frac{\overrightarrow{E} \times \overrightarrow{B}}{B^2} \rightarrow E_z = \frac{V_{DII}(1 + \Psi_0)B^2}{\sin(\Theta)H},$$ (3)

where Θ is the zenith angle of the radar beam, B is the Earth's magnetic field flux density, and H is its horizontal component. Finally, the E_y component is obtained by equation (4):

$$E_y = \frac{\int_{-\theta}^{+\theta} \sigma_P \mathbf{r} . d\theta}{\int_{-\theta}^{+\theta} \sigma_H \mathbf{r} . d\theta} E_z,$$ (4)

where r is the position of the magnetic field line element considering dipole geometry, θ is the magnetic latitude, $d\theta$ is the differential magnetic latitude element vector, and the integrals are the well-known

field line-integrated Pedersen and Hall conductivities, usually represented by Σ_P and Σ_H, respectively. The variables Ψ_0, Σ_P, and Σ_H are calculated by an ionospheric conductivity model extensively discussed recently by Moro et al. (2016c).

The E_y and E_z components inferred from RESCO data acquired on 7 February 2001 (a geomagnetic quiet day) are selected as a reference day in this work. The main features of these reference fields are the following: E_y shows a diurnal variability that varies from 0.01 to 0.38 mV/m, with mean equal 0.22 ± 0.05 mV/m, and the E_z component varies from 0.75 to 15.39 mV/m, with mean equal 8.85 ± 2.15 mV/m.

2.2. Ionospheric Data Collection and MIRE Model

We have used data from a digital ionosonde (Digisonde) installed at SLZ to collect the E_s parameters during the November 2004 geomagnetic storm. The Digisonde operates continuously, and electron density profiles are taken every 10/15 min with the sounding frequencies ranging from 1.0 to 30.0 MHz, with 0.5 MHz frequency step.

In order to identify the E_s layers, we use the ionograms provided by the Digisonde. Under the strong influence of the EEJ, it is possible to observe the Es_q layers most of the time. However, in some circumstances, the Es_b layer takes place, or both layers occur in the same period. In summary, both types of E_s layers (Es_b and Es_q) can be present at the same time depending on the EEJ current and electric field behavior. For details about these competitions of Es_b and Es_q, see Resende et al. (2016).

The Es_q and Es_b are simulated with the MIRE (Portuguese acronym for E region ionospheric model) model and compared with the ionograms. The MIRE model was originally developed by Carrasco, Batista, and Abdu (2007) and modified by Resende et al. (2017) with the purpose to simulate the ionospheric E region and the blanketing sporadic E layers. Specifically, this model computes the densities of the ions NO^+, O_2^+, N_2^+, O^+, Fe^+, and Mg^+, using numerical algorithms to solve a system of differential equations obtained from the continuity and momentum equations. Finite difference technique is applied to the differential equations, and these discretized results are solved using Crank-Nicholson method. The grid spacing used in the model is 0.05 km in the heights from 86 to 140 km with 2 min time step between 00:00 and 24:00 UT. All the input measurements used in this model, as the atmospheric and temperature parameters, collision frequency, and the iron and magnesium profiles, as well their seasonal variation, are explained by Carrasco et al. (2007) and Resende et al. (2017). The electron density n_e is given by equation (5):

$$n_e = \left[O_2^+\right] + \left[NO^+\right] + \left[O^+\right] + \left[N_2^+\right] + \left[Fe^+\right] + \left[Mg^+\right]. \tag{5}$$

The E_s layer formation depends mainly of the dynamical processes. Therefore, the vertical ion velocity (V_{iz}) shown in equation (6) describes the vertical transport, and it is used for each of the E region constituents. Using a coordinate system with the x axis pointing southward, the y axis westward, and the z axis upward, the V_{iz} equation is given by:

$$V_{iz} = \frac{\Omega_i^2}{\left(v_{in}^2 + \Omega_i^2\right)} \left[\cos I \sin I\, U_x + \frac{v_{in}}{\Omega_i} \cos I\, U_y + \frac{1}{v_{in}} \frac{e}{m_i} \cos I \sin I\, E_x + \frac{e}{\Omega_i m_i} \cos I\, E_y + \frac{e}{v_{in} m_i} \left(\frac{v_{in}^2}{\omega_i^2} + \sin^2 I\right) E_z\right], \tag{6}$$

where v_{in} and Ω_i are the ion-neutral collision frequency and ion gyrofrequency (described in equation (2)), respectively; I is the magnetic inclination angle; m_i represents the ion mass; e is the electric charge; E_x, E_y, and E_z are the electric field components; and U_x and U_y are the horizontal wind components in the southward (meridional) and eastward (zonal) directions, respectively.

Notice that the V_{iz} is a function of wind and electric field parameters. A vertical shear in this velocity is fundamental for E_s layer formation; that is, the E_s layers are formed at heights where the velocity is null. Thus, the competition between tidal winds and electric fields can be analyzed in the Es_b layer formation, which provides essential information about the equatorial E region electrodynamics. Regarding the tidal winds, the MIRE model was modified from its previous version by adding a novel theoretical neutral wind model that was obtained using the wind measurements acquired from the all-sky meteor radar at São João do Cariri (SJC, 7.4°S, 36.5°W, ~−10° dip angle), in the low-latitude Brazilian sector (Buriti et al., 2008). SJC is the nearest site to SLZ (where there is no wind data available) with an all-sky meteor radar, as shown in Figure 1. The
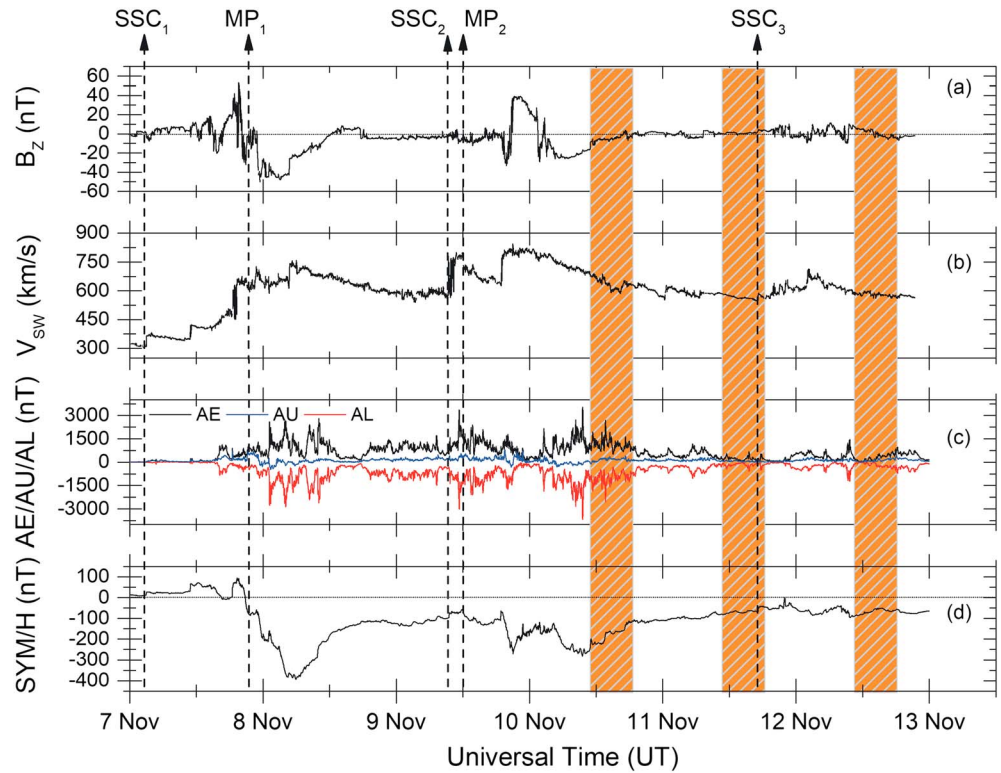
Figure 2. IMF B_Z, solar wind speed, *AE/AU/AL* auroral electrojet and *SYM/H* indices versus UT from 7 to 12 November 2004 geomagnetic storm.

inclusion of wind measurements to correctly describe the wind dynamics in the Brazilian region was implemented in the current version of MIRE model by a recent work of Resende et al. (2017). In summary, we have used the wind shear equations obtained by Mathews and Bekeny (1979) using the zonal and meridional, diurnal, and semidiurnal tidal wind components measured by the meteor radar. We have tested the global scale wave model and the horizontal wind model, but the models failed to simulate the formation of E_s over northeastern Brazil, which is a region with peculiar electrodynamic characteristics as described before.

2.3. Interplanetary Parameters

Finally, a complete set of data was used to characterize the storm time, its probable cause, and its effects in the Earth space environment. The IMF B_Z component (in nT) and solar wind speed V_{SW} (km/s) were taken from the OMNIWeb database obtained from the Advanced Composition Explorer (ACE) satellite measurements and are referred to the GSM coordinates system. The auroral electrojet *AE* (*AU/AL*) and the symmetric component of ring current (*SYM/H*) geomagnetic indices (in nT), which can be regarded as a high-resolution version of the *Dst* index, come from the World Data Center from Geomagnetism, Kyoto.

3. Results and Discussions

3.1. Interplanetary and Geomagnetic Disturbance Conditions During 7–12 November 2004

The time variations of the interplanetary magnetic field (IMF) B_Z component and solar wind speed (V_{SW}, km/s); *AE*, *AU*, and *AL* auroral electrojet indices (nT); and the *SYM/H* index (nT) for the 7–12 November 2004 geomagnetic storm are shown in the panels descending from the top of Figure 2. Although we are showing the 6 day storm, in this work, we will focus on the shaded areas only, which indicate the diurnal variation of E_y and E_z inferred with RESCO data during the recovery phase of the geomagnetic storm. Our intention with Figure 2 is to provide a comprehensive view of the complex geophysical conditions during the storm time analyzed here.
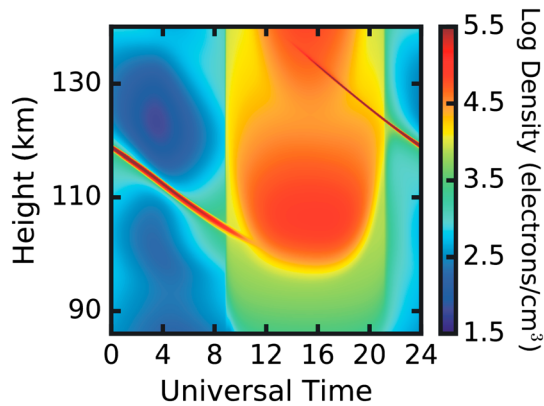
Figure 3. Electron density as a function of universal time (UT) and height (km) simulated by MIRE considering the diurnal and semidiurnal tidal winds representative of November 2004.

Two coronal mass ejections (CMEs) hit the Earth's magnetosphere between 7 and 10 November 2004 producing a super double (and rare) magnetic storm in a period of declining phase of solar flux, with a daily $F_{10.7}$ index of about 130 ($\times 10^{-22}$ Wm^{-2} Hz^{-1}). The CME cloud hitting the Earth on 7–8 November produced the first of the two super storms observed in the panel of the SYM/H index. The storm sudden commencement (SSC$_1$) occurred at 02:57 UT, and the onset of the storm main phase (MP$_1$) occurred at 21:30 UT on 7 November, as indicated by the vertical dashed lines identified with the "MP$_1$" mark. The ACE spacecraft measured abnormally large B_Z (Figure 2a) variations, up to about 50 nT, on this day. The solar wind speed (V_{SW}, Figure 2b) increased gradually from about 330 km/s to more than 700 km/s. In the following day, the AE index (Figure 2c) reached values higher than 2,500 nT between 01:10 and 10:12 UT. On 8 November, the activity reached the top of the geomagnetic K-scale measurement (not shown here) during 03:00–06:00 UT, and the lowest intensity of SYM/H index (Figure 2d) with values around −400 nT was observed at 05:55 UT.

The second CME cloud struck the magnetosphere on 9 November, while the magnetic field was experiencing the first recovering phase of the first storm, as can be noted in Figure 2d. The second SSC$_2$ occurred at 09:30 UT on 9 November, characterized by an increase in the solar wind speed from about 550 km/s to 800 km/s, concomitant with large oscillations in the AL/AU values. The MP$_2$ onset of this second storm occurred at 12:00 UT, as shown by the vertical dashed line identified with the "MP$_2$" mark. The southward turning of the B_Z was also responsible for a prompt onset of an AE intensification to values >3,200 nT at 11:20 UT on 9 November, and a secondary minimum of about −270 nT was registered by the SYM/H at 21:03 UT. After a short recovery period, the SYM/H reached −282 nT at 09:31 UT on 10 November, which is characterized by a large intensification of AE up to 3,534 nT (maximum value observed during this geomagnetic storm). Later, during the recovering period of the geomagnetic storm, on 11 November, the solar wind speed gradually decreased to about 600 km/s, and the SYM/H achieved −50 nT when another SSC$_3$ was registered at 17:10 UT. We may note that B_Z was positive at this SSC$_3$ occurrence and reversed to south at 22:54 UT while the V_{SW} and AE index kept growing until around 11:00 UT on 12 November, returning back to quiet time values in the next hours.

During this major geomagnetic storm, the equatorial ionospheric electric fields experienced significant deviations from their quiet time patterns. The modification of the electric fields can occur mainly owing to two mechanisms: prompt penetration electric field (PPEF) (Kikuchi et al., 2000) and disturbed dynamo electric fields (DDEF) (Blanc & Richmond, 1980). The role of these two mechanisms regarding our results will be discussed later. We can anticipate that the strongest PPEF ever reported (from the best of our knowledge) was observed during this geomagnetic storm, at 20:00 UT (15:00 LT) on 9 November at JRO, which caused a vertical drift velocity of 120 m/s (Fejer et al., 2007).

3.2. The Role of E_y and E_z Components in the Es$_b$ and Es$_q$ Electrodynamics

Figure 3 shows the height-time-intensity (HTI) map of E region electron density profile simulated with the MIRE model considering only the wind components representative of November 2004 over SLZ. Note that n_e given in cm^{-3} is based on the plasma frequency relationship by $n_e = 1.24 \times 10^4 (f_bEs)^2$. We observed a typical behavior of the E region electron density, with low values in the night period and expressive electron density in the daytime. Also, it is possible to identify a thin layer of enhanced electron density that is the Es$_b$ layer. In this result, the Es$_b$ is formed above 130 km around 14:00 UT and descends to 100 km at 08:00 UT with expressive values. The downward movement of Es$_b$ is due to the well-defined regularity in both semi diurnal and diurnal tidal winds during the course of the day, as explained by Haldoupis (2011). Therefore, the input wind shear in MIRE model successfully simulated the Es$_b$ layer evolution over SLZ (Resende et al., 2017).

In order to analyze the effect of the electric field components in the Es$_b$ dynamics during the geomagnetic storm, the E_y and E_z components inferred at 105.1 km from RESCO data are inserted into equation (6). The discussions about the effects of E_y and E_z components in the simulations of the Es$_b$ dynamics by MIRE
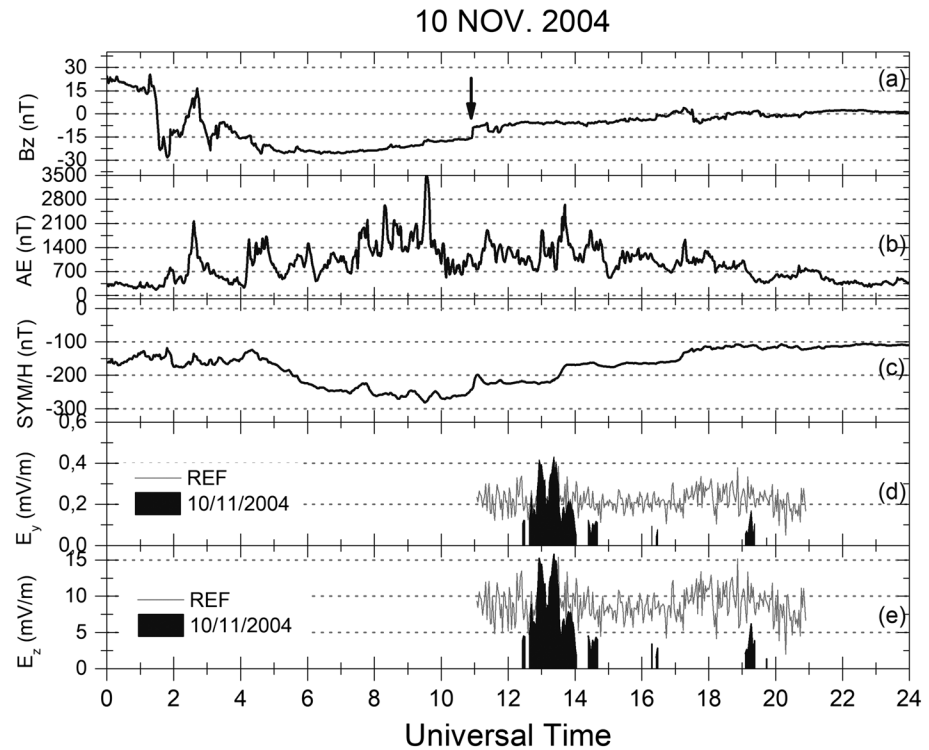
Figure 4. Diurnal variation of the (a) IMF B_Z component, (b) AE index, (c) SYM/H, (d) E_y, and (e) E_z on 10 November 2004.

model during two geomagnetic quiet periods, 5 January 2005 and 13 December 2009, are shown by Resende et al. (2016). In the following, we discuss three cases of the EEF and E_s layer responses to the recovery phase of the November 2004 geomagnetic storm.

3.2.1. Case I: 10 November 2004—Weak Type II Irregularities and Strong Es_b Occurrences

After showing the whole geomagnetic storm period (7–12 November 2004) in Figure 2, we analyze in more details the diurnal variation of the electric field components and E_s dynamics observed on 10 November 2004. We consider the electric fields inferred from RESCO data as an input of the MIRE model, with the tidal winds used to build the electron density profile shown in Figure 3. First, we present from top to bottom in Figure 4 the diurnal variation of the (a) IMF B_Z component, (b) AE index, (c) SYM/H index, (d) E_y, and (e) E_z, respectively. The gray lines in Figures 4d and 4e are the electric field components corresponding the quiet period that we have used as a frame of reference, as described in section 2.1.

As mentioned before, 10 November 2004 was marked by a complex period of magnetic activity caused by successive increases and decreases of magnetospheric convection. This characteristic is seen in more details in Figures 4a–4c. The IMF B_Z turned south at 01:31 UT and achieved −29 nT at 01:49 UT. Thereafter, it increased up to turn itself northward with a pick of 16.72 nT at 02:42 UT. Afterward, it remained negative for several hours until 16:53 UT. In this period, a series of large enhancements and recovery of AE were observed. The AE index reached values of the order of (and higher than) 1,000 nT for a long period of time (between 02:30 and 19:00 UT), rising to higher than 3,000 nT. The maximum intensity of 3,534 nT in AE occurred at 09:34 UT. The SYM/H remained below −100 nT during the whole day with a minimum value of −282 nT registered at 09:31 UT. Therefore, the equatorial ionosphere over SLZ was exposed to the influence of the enhanced dawn-to-dusk convection electric field around local midnight (UT-3), but mostly post midnight. As a consequence, an undershielding PPEF of westward polarity persisting in the morning hours caused a weakening in the EEJ, which led the 3 m irregularities to not develop until before 12:20 UT. Richmond, Peymirat, and Roble (2003) pointed out that the shielding effect is established with a characteristic time scale of the order of 3–300 min depending on magnetosphere plasma properties and ionospheric conductivity. After an extended period of B_Z south, which lasted until around 11:00 UT, it suddenly turned northward, associated with an increase of AE. This condition created an overshielding electric field such that the

net equatorial electric field associated with direct penetration reversed direction to eastward. As a result, a short duration of Type II patch near 12:30 UT to 14:00 UT was observed in RESCO radar data, which is caused by a rapid decrease in the magnetospheric convection, leading to the reestablishment of the shielding. This process started around 11:00 UT, which is indicated in Figure 3a by the arrow.

After detecting the Type II development, we were able to infer both electric field components and compare them to the "quiet days" (gray lines in Figures 3d and 3e from Moro et al., 2016c). Two peaks higher than 0.40 mV/m in the E_y component between 12:30 UT and 14:00 UT are observed. Since the E_y is obtained from the E_z component along with the field line integrated Pedersen and Hall conductivity ratio (see equation (4)), two peaks are also seen in E_z. They are both higher than 15 mV/m. From the electric fields, one can note that we have the information about intermittent Type II occurrences at around 14:30 UT, 16:30 UT, and 17:00 UT. The low intensities in E_y and E_z are related to the low velocity of the Type II irregularity (see equation (3)) at these periods of time. These peaks are lower than 0.20 mV/m in the E_y component and around 5.00 mV/m in the E_z component. Anyway, both E_y and E_z components are lower than the reference components. This is an evidence of the electric field intensity decreasing associated with Type II disappearance due to the storm time changes under B_Z south condition and associated with AE increases. As far as we know, this is the first result showing the equatorial E region electric field during a geomagnetic disturbed day, inferred from coherent radar data. We also show the diurnal variation of these components on 11 and 12 November 2004, which will be discussed later.

The ionograms obtained at SLZ when the estimated electric fields presented low or zero intensity values, from 15:00 to 20:45 UT, are presented in Figure 5. In each ionogram, the scales range from 0 to 500 km in altitude (vertical axis), and from 0 to 15 MHz (horizontal axis). The red arrows in this figure identify the Es_q layers, while the black arrows identify the Es_b layers. As can be observed, the Es_b layers occurred only between 16:00 UT and 20:45 UT. The black vertical line represents the parameter that refers the upper frequency to which the upper ionosphere region is blocked by the Es_b layer. Therefore, since the Es_q layer is transparent to the radio waves, it is not possible to obtain the blanketing frequency of the E_s layer (fbEs) when it is present.

It is possible to observe in the ionograms a direct response of the prompt penetration of the high-latitude electric field events (Gonzales et al., 1979) to the E region (Abdu et al., 2013). The Es_q layer is a clear evidence of the EEJ irregularity, in whose presence the entire F layer trace can be observed in ionograms as it is shown at around 15:00 UT and 15:15 UT. At 15:30 UT we start to observe another type of E_s layer above the Es_q layer. It was not so expressive at this time, but it was dense enough to start blocking the F region (fbEs ≈ 3.87 MHz) from the ionosonde radio soundings. This blanketing layer became evident at 16:00 UT (black arrow) when the fbEs parameter reached 4 MHz (vertical black trace). Since the parameter fbEs is a measure of the plasma frequency of the E_s layer peak density, we observe that from this hour, the Es_b layer becomes denser. The fbEs parameter reached values around 4.86 MHz at 17:15 UT. From 16:00 UT to 17:15 UT the Es_q layer became weaker than usual but did not disappear, indicating the presence of long-scale plasma irregularities. At 17:30 UT, we observed that both Es_b and Es_q layers revealed a competition between two different driving mechanisms, winds, and electric fields. At 18:15 UT, the Es_q layer disappears and the Es_b layer dominated in the ionogram at the E region. Afterward, a different layer was registered in height altitudes ≈250 km and it performed a downward movement until 20:15 UT, when it reached 100 km. In the hours that followed, a strong Es_b layer was formed, evidencing the weakness of the EEJ current around the nighttime period.

The occurrence of the Es_q and Es_b layers reveals the importance of the electric field role during the disturbed periods. We observed that during the recovery phase of the magnetic storm the Es_b layers were stronger after 16:00 UT, and the E_y and E_z showed really low values at around 16:15 UT. Additionally, the Es_q layer did not occur around between 18:15 UT and 19:15 UT, when we observed lower values in the electric field components. Thereafter, we observed a peak in the E_y and E_z components with intensity above 5 mV/m, and the Es_q layer started to be formed again (20:00 UT).

The weakness of the EEJ current seen in the electric fields occurred in the recovery phase of the magnetic storm, which was proved by the Es_q disruption/Es_b formation in the ionograms. This fact evidences that the reversal of E region horizontal electron drifts, which, in turn, means an imposition of a westward ionospheric electric field, which occurred at the same time that the IMF B_Z changed from its southward to
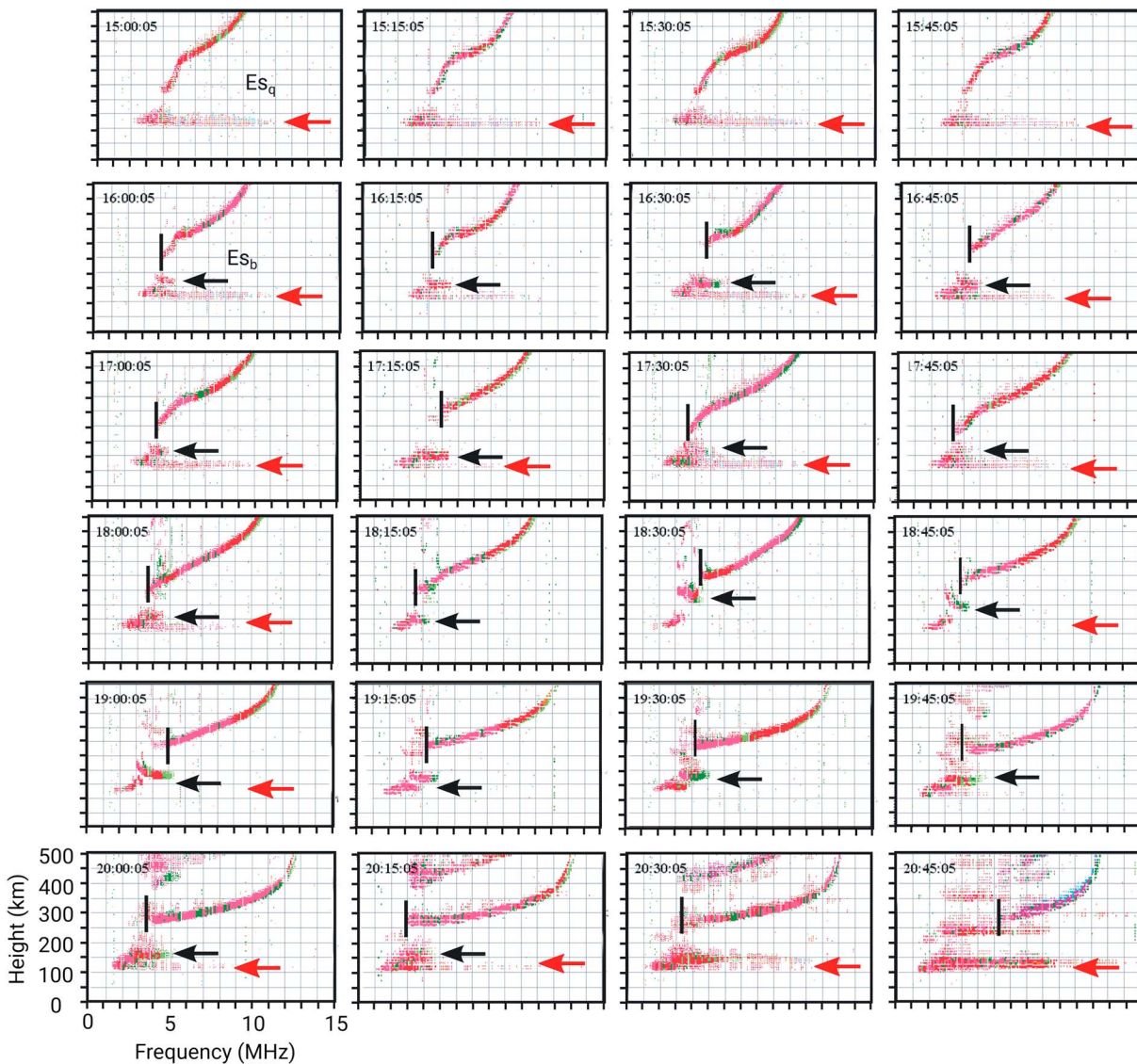
Figure 5. Ionograms collected by a Digisonde at SLZ on 10 November 2004, from 15:00 UT to 20:45 UT. The red (black) arrows indicate the presence of Es_q (Es_b) layers. The reflections of ordinary and extraordinary waves are red and green, respectively.

northward direction. An additional evidence to support our statement is the intermediate layer presence at around 18:00 UT, which means stronger winds than electric fields in the E_s layer formation.

In order to analyze the geomagnetic storm effects in the equatorial E region in a more comprehensive way, we show the HTI maps of the E region electron density profile simulated by MIRE model (color scale) considering the winds with the zonal electric field, winds with the vertical electric field, and winds with both electric field components on 10 November 2004 (Figure 6). Notice that we have used the same input winds shown in Figure 3. This is acceptable due two reasons: we are using tidal winds representative of entire November 2014, and second, the winds have no expressive day-to-day variation. Since the EEJ current is not effective at nighttime, it is possible, therefore, to evaluate in these maps the influence of winds and electric fields on the E_s formation or disruption process during the disturbed period. The E_y and E_z inputs in these simulations are the components presented in Figures 4d and 4e.

The evolution of the E region electron density taking into account the tidal winds and E_y shows that the Es_b layer shall appear during all day long, as per the MIRE simulations. This result is similar to the result presented in Figure 3. This result agreed with the previously published results for quiet time periods obtained by Resende et al. (2016). Therefore, E_y is not efficient enough to create or disrupt Es_b even during a period of
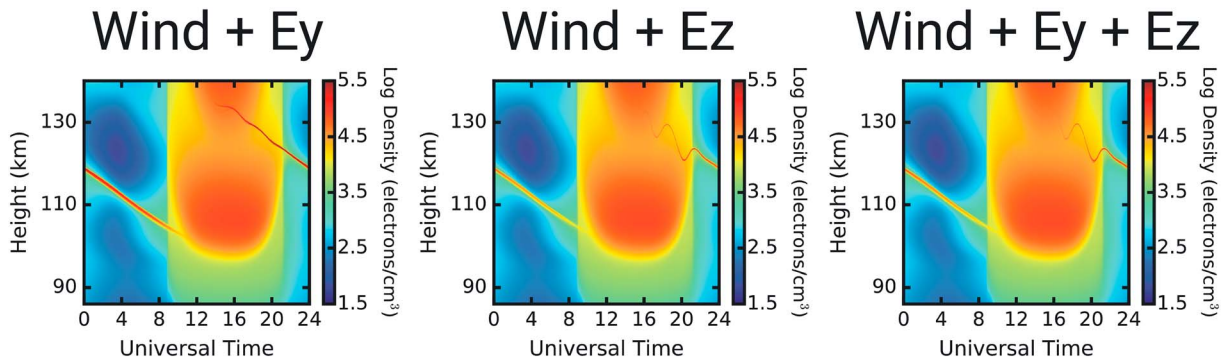
Figure 6. Electron density as a function of time (UT) and altitude (km) simulated by MIRE for 10 November 2004 considering the tidal winds with the zonal electric field component (E_y), the vertical electric field component (E_z), and both zonal and vertical electric field components ($E_y + E_z$).

geomagnetic activity. However, we observed a smooth modulation between 11:00 UT and 16:00 UT. We notice from the results in Figure 4d that the E_y component shows oscillations between low and the reference values, showing that the model reacts well to this behavior. It is possible that the zonal electric fields may be responsible for a modulation in the existing Es_b layers due to tidal winds, as shown in Dagar et al. (1977). On the other hand, when we consider the wind and the E_z component, we have a clear disruption of Es_b in some hours. Before 09:00 UT, the simulated Es_b layer occurs with the downward movement characteristic, which is caused by a downward movement due to the semi diurnal tidal phase at altitudes around 135–150 km (Harper, 1977). After 21:00 UT, the same behavior occurs.

In a typical day, when the E_z component is very high during the daytime, the MIRE does not successfully simulate the Es_b layer (Resende et al., 2016). However, in the present result, the Es_b layer becomes evident after 15:30 UT. This model result is supported by the ionosonde observations provided in Figure 5, and by low values of the E_z component (around 3.0 mV/m), as seen in Figure 4e. Therefore, we may state that the E_z effect is more relevant to the EEJ dynamics during the disturbed periods based on the present analysis.
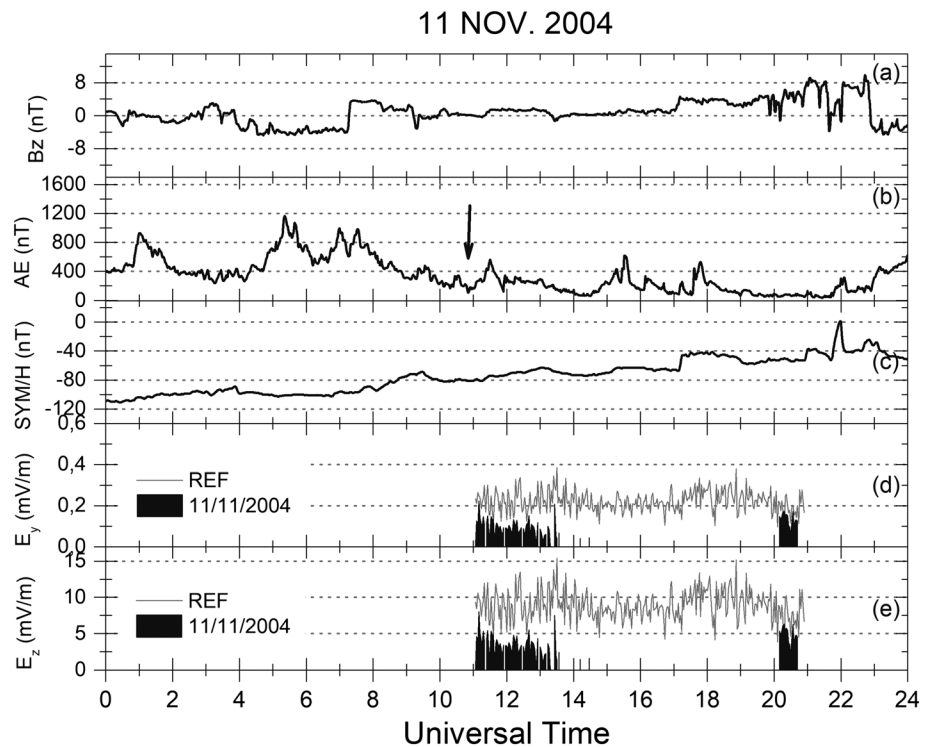

Figure 7. IMF B_Z component, AE index, SYM/H, and E_y and E_z components on 11 November 2004.

The simulation results showed several oscillations that we do not observe in ionograms (especially at around 18:30). However, we do observe oscillation-like behavior in the electric field amplitude variation. Consequently, we understand that these modulations in the simulation results are a real effect of the combination of E_y and E_z inputs in the model. In theory, the Es_b layers due to the tidal winds are formed at high altitudes (above 130 km) and descend to below 100 km (Harper, 1977). We clearly observe this evidence after 18:30 UT in the ionograms, and the MIRE simulations agreed with this behavior. Similar behavior was also observed on the ionograms in midlatitudes (Bishop & Earle, 2003; Haldoupis et al., 2006), in which the electric field does not cause any influence in the E_s layer formation. Therefore, this result confirms that the wind effects were more effective than the electric field effects over SLZ. Finally, when we included both E_y and E_z electric field components superimposed to the effects of the tidal winds in the simulation, we observed similar results to those considering only the vertical electric field component. As explained by Resende et al. (2016), the vertical electric field is the most important component for the Es_b layer formation in the latitudinal range, in such a way that Es_b layer only occurs under low values of E_z.

3.2.2. Case II: 11 November 2004—Very Weak Type II Irregularities and Es_b Occurrences

On similar lines as those of Figure 4, Figure 7 shows the IMF B_Z component, AE index, SYM/H index, and the diurnal variation of the E_y and E_z with corresponding quiet time values used as a reference. Successive intensifications in the AE index are observed at 01:00 UT, 05:15 UT, and between 07:00 and 08:00 UT on 11 November when it achieved around 1,000 nT. One could notice that the intensification of the AE index close to ~500 nT (as indicated by the black arrow in Figure 7b) at 11:00 UT produced very weak Type II irregularities almost at the same time until 13:30 UT. On the other hand, through the occurrence of very large DDEF due to lower latitude thermospheric winds (Fejer et al., 2007), the main effect on the EEJ was the absence of any irregularity development from around 13:30 UT to 20:00 UT.

We observe in the results of Figure 7d that E_y presented two peaks higher than 0.20 mV/m. The first one occurred at around 11:10 UT, and the second was registered at around 13:20 UT. The two peaks are also observed in the E_z component, which achieved around 7.50 mV/m. Except for these peaks, both components show lower intensity than the reference components. The SSC_3 at 17:10 UT (see Figure 2) and accompanying transient increases and decreases in B_Z, and AE appears to have caused the generation of short-lived Type II after 20:00 UT due to a PPEF of eastward polarity.

A series of ionograms recorded on 11 November at SLZ is shown in Figure 8 and follows the same patterns of those presented in Figure 5. Here we have selected the ionograms collected from 10:00 UT to 14:45 UT, which we considered to be enough to analyze the time evolution and occurrence of the Es_q (Es_b) layers represented by red (black) arrows. Recalling that the Es_b layers occur above the Es_q layer and they block the Digisonde signal from the F region (black vertical trace), it is blocked up to around 4 MHz on this period of analysis.

The HTI maps of the E region electron density simulation results obtained from the MIRE over SLZ on 11 November are shown in Figure 9. They follow the same patterns of Figure 6. From the simulation result obtained when considering the wind and E_y component as the driving forces, we clearly see the thin electron density enhancement at different heights during all day depicting the Es_b layer. This thin layer is seen above 130 km (at ~14 UT), which descends to around 100 km (at ~10 UT), and is even stronger than that observed in the previous simulation runs for 10 November.

Again, a disruption is seen when we consider the winds and E_z component in the simulation. Indeed, we expected this since the intensity of E_z on November 11 was higher than 3.85 mV/m, the threshold value for disrupting the Es_b layer as stated by Resende et al. (2016). During some daytime hours, the density of the Es_b layer was very close to the E region peak density, making it difficult to identify the Es_b trace. When the simulation is run considering the wind and both electric field components, we have the same situation as the day before; that is, the E_y component is not important for Es_b development/inhibition. Therefore, during the hours that the wind shear mechanism was more effective than the irregularities, it was possible to observe the Es_b layer in the simulations.

3.2.3. Case III: 12 November 2004—Strong Type II and Weak Es_b Occurrences

Similarly to the Figures 4 and 7, Figure 10 shows the IMF B_Z component, and AE and SYM/H indices of our last case in this study, 12 November. The southward turning of IMF B_Z followed by AE intensification between 09:00 and 10:00 UT caused the PPEF with eastward polarity. The E_y and E_z electric field components closely match their quiet time values given by the reference components, as shown in Figures 10d and 10e.
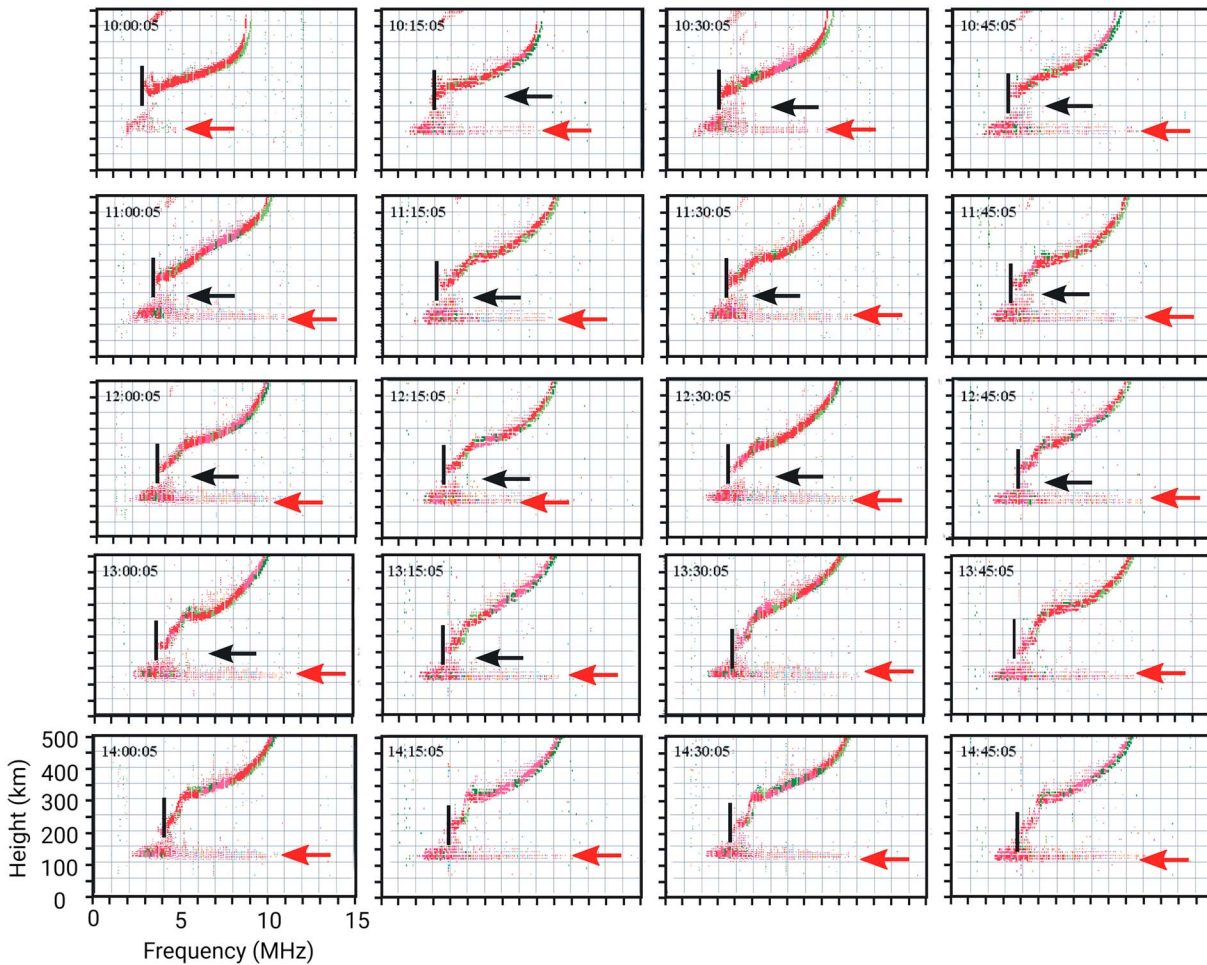
Figure 8. Ionograms collected by a Digisonde at SLZ on 11 November 2004, from 10:00 UT to 14:45 UT. The red (black) arrows indicate the presence of Es_q (Es_b) layers. The reflections of ordinary and extraordinary waves are red and green, respectively.

Under this environment, the Type II irregularities were presented during the radar soundings from 11:00 UT to 20:45 UT, allowing the electric field inference. The E_y ranged from 0.10 to 0.39 mV/m, and E_z ranged from 3.00 to 14.50 mV/m. Both electric field components were still weaker than the reference values but could sustain the gradient instabilities generation of 3 m scale size irregularities giving backscatter returns during the radar soundings. Therefore, we expect the presence of the Es_q in the ionograms collected at SLZ indicating the presence of Type II irregularities.

Figure 9. Electron density as a function of time (UT) and altitude (km) simulated by MIRE for 11 November 2004.
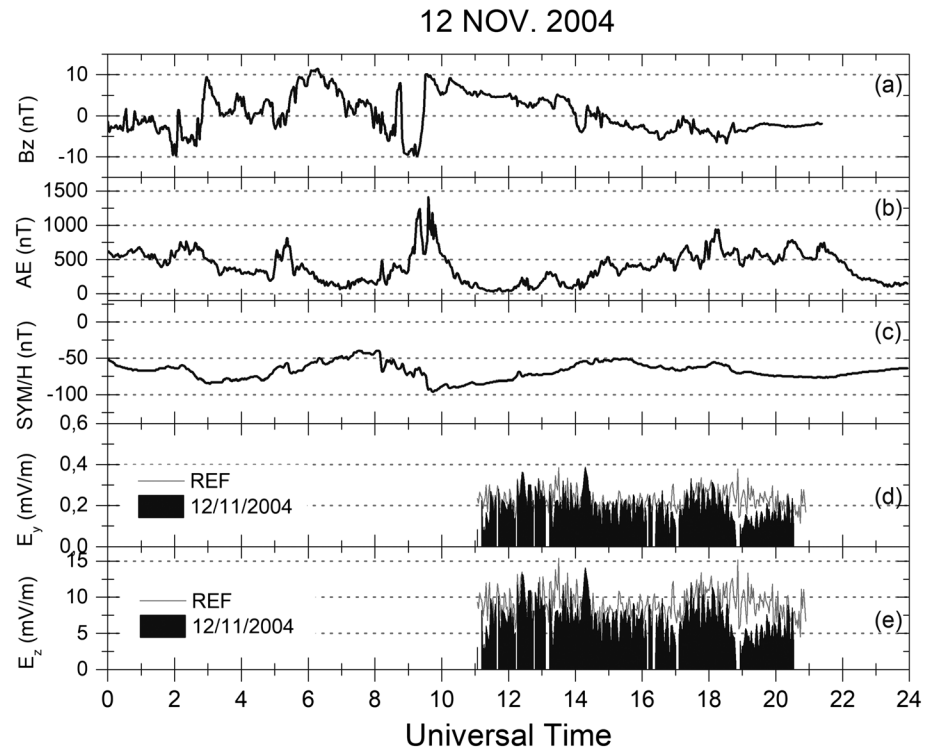
Figure 10. IMF B_Z component, AE index, SYM/H, and E_y and E_z components on 12 November 2004.

The sequence of ionograms collected at SLZ on 12 November is presented in Figure 11 and follows the same patterns of those presented in Figures 5 and 8. Now we have selected the ionograms acquired from 15:00 UT to 19:45 UT. Besides not shown here, the Es_b layer appeared weak in the ionograms since 10:30 UT and became more evident at 15:15 UT, as shown in Figure 11.

The Es_q layer is evident in the ionograms most of the time (through 15:00 UT to 19:45 UT), allowing the electric field inference as discussed before. On the other hand, the Es_b layers appeared weak in the ionograms. In addition, the fbEs blocked the F region at around 4 MHz between 15:00 UT and 16:30 UT. After this period, the F region completely appears in ionograms, and a remnant of the Es_b layer continues to appear in the ionograms after 16:30 UT, but it is very weak. In fact, in this case, the E_s layer is partially blocking the upper layers, in which it is observed through the absence of trace curvature at the lower frequency end of the F layer. Therefore, the process responsible for Es_q layer formation, that is, electric field, was stronger than wind shear processes that give rise to the Es_b layer.

The HTI maps of the E region electron density simulated with the MIRE over SLZ on 12 November are shown in Figure 12. The simulation conducted considering only wind components and E_y shows a clear electron density enhancement from 9:00 UT above 130 km descending to around 100 km, similar to the previous days. In the run considering wind components and E_z, we note a weak presence of Es_b, as also confirmed in the ionograms. If we compare this result with the previous day, 11 November, we can also note that the Es_b is inhibited due to the presence of stronger Es_q layer. The last simulation considering the winds and both electric field components shows results similar to that of Figure 9; that is, it is evident that the E_y does not affect the Es_b dynamic process.

The results presented in this work show a persistent disturbance in the EEJ plasma irregularities during the recovery phase of the geomagnetic storm, lasting for approximately 48 h. Thus, this study was able to prove such influences through of the Es_b and Es_q layer occurrences. The Es_q layer weakness is related the E_z component, which presents low values during the disturbed periods. So in these times with the low values of the E_z component, the Es_b layer can occur due the wind process. The wind shear can be effective in the Es_b formation over SLZ region because of the magnetic equator displacement effect.
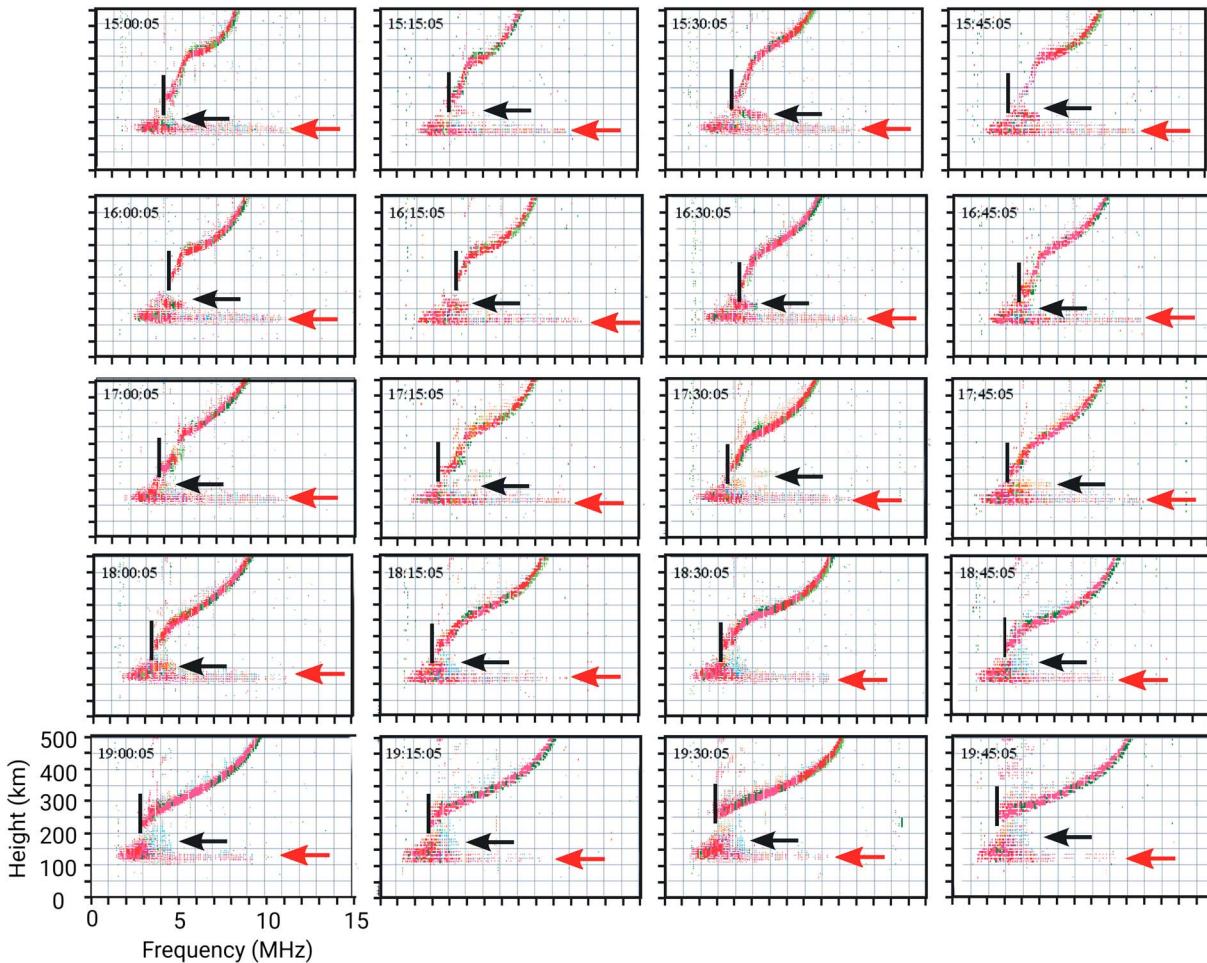
Figure 11. Ionograms collected by a Digisonde at SLZ on 12 November 2004, from 15:00 to 19:45 UT. The red (black) arrows indicate the presence of Es_q (Es_b) layers. The reflections of ordinary and extraordinary waves are red and green, respectively.

Several studies have been made to study the November 2004 response to space weather events, with focus on the F region responses to PPEF and DDEF. No study has so far been reported on the response features of the equatorial E region to the disturbance electric fields as we present in this work. For instance, Balan et al. (2008) studied the magnetosphere-ionosphere coupling through PPEF during on 7 November 2004 using the Cluster satellite data and ground-based data obtained from the EISCAT Svalbard radar (78.15°N, 16.0°E), EISCAT UHF radar (69.67°N, 19.20°E), JRO radar, and magnetometers (World Data Center, Kyoto). The authors
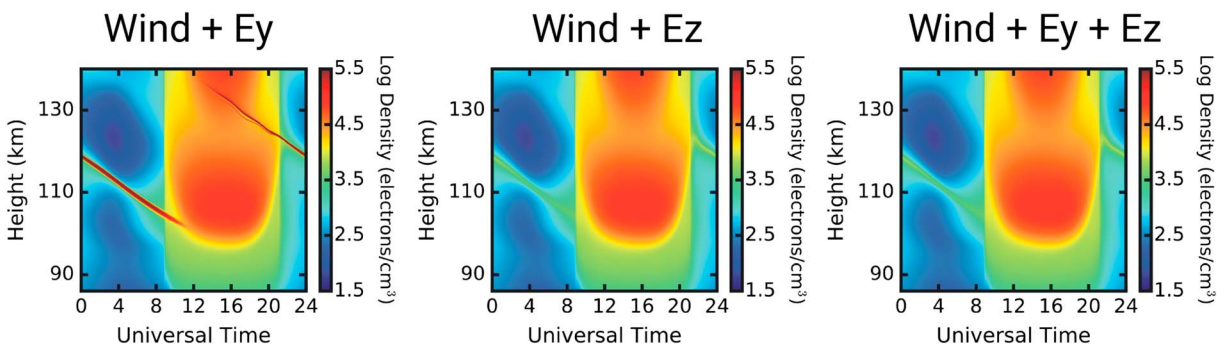

Figure 12. Electron density as a function of time (UT) and altitude (km) simulated by MIRE for 12 November 2004.

observed an increased ionization production by particle precipitation, which increased the electron density and electron and ion temperatures. An anomalous total electron content (TEC) enhancement was observed by Maruyama (2006) on 8 November 2004 using a dense GPS receiver network at longitudes of Japan. The storm enhanced density, until then observed only at longitudes of America due to geomagnetic field configuration (Foster, 1993), was observed in the Asia sector appearing to move at a rate of 8°/h with a signature of PPEF. Vijaya Lekshmi et al. (2008) have shown the relative effects of the main drivers of the positive ionospheric storm under PPEF to eastward and direct and indirect effects of equator ward neutral wind using the Sheffield University Plasmasphere Ionosphere Model. Li et al. (2009) analyzed the development and dynamics of ionospheric plasma bubble irregularity during this super storm using data from a multi instrument network (GPS TEC, ionosonde, GPS scintillation) operated in Southeast Asia. More recently, Rastogi et al. (2012) showed cases of strong E_s layer formation on 9 November 2004 in India sector due to abnormally large equatorial prompt penetration dawn to dusk electric field.

Finally, in this work, we studied the E region phenomenology during a super geomagnetic storm. We observe that the electric fields present in the equatorial E region can generate plasma irregularities that can act as scattering centers for radar sounding and are seen in ionograms as Es_q traces. On the other hand, the peculiar geomagnetic characteristic over the SLZ region, a quasi-equatorial station where the magnetic declination angle is ~21°W (and the magnetic inclination varies at a rate of ~20′ per year causing the dip equator secular displacement effect), allows the appearance of the Es_b layers. The vertical component, E_z, can inhibit the formation of the Es_b layers, as predicted by the model results. All cases discussed here showed that E_z is more important in the EEJ dynamics in SLZ region than the zonal component of the electric field.

4. Conclusions

We have performed a comprehensive study of the variabilities of the zonal (E_y) and vertical (E_z) electric field components inferred from coherent radar data, during the super storm of November 2004. The E_s layers observed from a Digisonde data and modeling results are also used to study the responses of the equatorial E region over SLZ, Brazil.

The features of the E region dynamo electric field, EEJ (and its plasma irregularities), and sporadic E layers are strongly affected by the geomagnetic storm. The results show that the electric field components are affected when the equatorial ionosphere is exposed to the influence of the enhanced dawn-to-dusk convection electric field causing the enhanced occurrence and suppressions of Type II irregularities. The short duration of Type II irregularities observed in some cases is associated with electric fields with lower intensity than the reference values. This scenario is favorable for the Es_b layer development, which we confirm from Digisonde data and modeling results. Therefore, we could show the efficiency of the wind system with the E_z decreasing over SLZ, Brazil. On the other hand, when the Type II irregularities develop during the recovery phase, the electric fields associated with its velocity are still lower than the reference values but intense enough to develop the Es_q layers seen in ionograms. In this case, the E_z is intense to disrupt the Es_b seen in the modeling results.

References

Abdu, M. A., Batista, I. S., Muralikrishna, P., & Sobral, J. H. A. (1996). Long term trends in sporadic E layers and electric fields over Fortaleza, Brazil. *Geophysical Research Letters*, *23*(7), 757–760. https://doi.org/10.1029/96GL00589

Abdu, M. A., Bittencourt, J. A., & Batista, I. S. (1981). Magnetic declination control of the equatorial F region dynamo electric field development and spread F. *Journal of Geophysical Research*, *86*(A13), 11,443–11,446. https://doi.org/10.1029/JA086iA13p11443

Abdu, M. A., de Souza, J. R., Batista, I. S., Santos, A. M., Sobral, J. H. A., Rastogi, R. G., & Chandra, H. (2014). The role of electric fields in sporadic E layer formation over low latitudes under quiet and magnetic storm conditions. *Journal of Atmospheric and Solar - Terrestrial Physics*, *115-116*, 95–105. https://doi.org/10.1016/j.jastp.2013.12.003

Abdu, M. A., Souza, J. R., Batista, I. S., Fejer, B. G., & Sobral, J. H. A. (2013). Sporadic E layer development and disruption at low latitudes by prompt penetration electric fields during magnetic storms. *Journal of Geophysical Research: Space Physics*, *118*, 2639–2647. https://doi.org/10.1002/jgra.50271

Balan, N., Alleyne, H., Walker, S., Reme, H., McCrea, I., & Aylward, A. (2008). Magnetosphere-ionosphere coupling during the CME events of 07–12 November 2004. *Journal of Atmospheric and Solar - Terrestrial Physics*, *70*(17), 2101–2111. https://doi.org/10.1016/j.jastp.2008.03.015

Batista, I. S., Abdu, M. A., & Bittencourt, J. A. (1986). Equatorial F region vertical plasma drifts: Seasonal and longitudinal asymmetries in the American sector. *Journal of Geophysical Research*, *91*(A11), 12,055–12,064. https://doi.org/10.1029/JA091iA11p12055

Batista, I. S., Diogo, E. M., Souza, J. R., Abdu, M. A., & Bailey, G. J. (2011). Equatorial Ionization Anomaly: The Role of Thermospheric Winds and the Effects of the Geomagnetic Field Secular Variation. In M. Abdu & D. Pancheva (Eds.), *Aeronomy of the Earth's Atmosphere and Ionosphere*, IAGA Special Sopron Book Series (Vol. 2). Dordrecht, Netherlands: Springer.

Bishop, R. L., & Earle, G. D. (2003). Metallic ion transport associated with mid-latitude intermediate layer development. *Journal of Geophysical Research*, *108*(A1), 1019. https://doi.org/10.1029/2002JA009411

Blanc, M., & Richmond, A. D. (1980). The ionospheric disturbance dynamo. *Journal of Geophysical Research*, *85*(A4), 1669–1686. https://doi.org/10.1029/JA085iA04p01669

Buriti, R. A., Hocking, W. K., Batista, P. P., Medeiros, A. F., & Clemesha, B. R. (2008). Observations of equatorial mesospheric winds over Cariri (7.4°S) by a meteor radar and comparison with existing models. *Annales de Geophysique*, *26*(3), 485–497. https://doi.org/10.5194/angeo-26-485-2008

Carrasco, A. J., Batista, I. S., & Abdu, M. A. (2007). Simulation of the sporadic E layer response to pre-reversal associated evening vertical electric field enhancement near dip equator. *Journal of Geophysical Research*, *112*(A6), A06324. https://doi.org/10.1029/2006JA012143

Cohen, R. (1973). Phase velocities of irregularities in the equatorial electrojet. *Journal of Geophysical Research*, *78*(13), 2222–2231. https://doi.org/10.1029/JA078i013p02222

Dagar, R., Verma, P., Napgal, O., & Setty, C. S. G. K. (1977). The relative effects of the electric fields and neutral winds on the formation of the equatorial sporadic layers. *Annales de Geophysique*, *33*(3), 333–340.

Denardini, C. M., Abdu, M. A., de Paula, E. R., Wrasse, C. M., & Sobral, J. H. A. (2006). VHF radar observations of the dip equatorial E-region during sunset in the Brazilian sector. *Annales de Geophysique*, *24*(6), 1617–1623. https://doi.org/10.5194/angeo-24-1617-2006

Denardini, C. M., Aveiro, H. C., Sobral, J. H. A., Bageston, J. V., Guizelli, L. M., Resende, L. C. A., & Moro, J. (2013). E region electric fields at the dip equator and anomalous conductivity effects. *Advances in Space Research*, *51*(10), 1857–1869. https://doi.org/10.1016/j.asr.2012.06.003

Denardini, C. M., Moro, J., Resende, L. C. A., Chen, S. S., Schuch, N. J., & Costa, J. E. R. (2015). E region electric field dependence of the solar activity. *Journal of Geophysical Research: Space Physics*, *120*, 8934–8941. https://doi.org/10.1002/2015JA021714

Devasia, C. V., Jyoti, N., Subbarao, K. S. V., Tiwari, D., Reddi, C. R., & Sridharan, R. (2004). On the role of vertical electron density gradients in the generation of type II irregularities associated with blanketing Es (Esb) during counter equatorial electrojet events: A case study. *Radio Science*, *39*, RS3007. https://doi.org/10.1029/2002RS002725

Fejer, B. G., Jensen, J. W., Kikuchi, T., Abdu, M. A., & Chau, J. L. (2007). Equatorial Ionospheric electric fields during the November 2004 magnetic storm. *Journal of Geophysical Research*, *112*, A10304. https://doi.org/10.1029/2007JA012376

Forbes, J. M. (1981). The equatorial electrojet. *Reviews of Geophysics*, *19*(3), 469–504. https://doi.org/10.1029/RG019i003p00469

Foster, J. C. (1993). Storm time plasma transport at middle and high latitudes. *Journal of Geophysical Research*, *98*(A2), 1675–1689. https://doi.org/10.1029/92JA02032

Gonzales, C., Kelley, M., Fejer, B., Vickrey, J., & Woodman, R. (1979). Equatorial electric fields during magnetically disturbed conditions: 2. Implications of simultaneous auroral and equatorial measurements. *Journal of Geophysical Research*, *84*(A10), 5803–5812. https://doi.org/10.1029/JA084iA10p05803

Haldoupis, C. (2011). A tutorial review on sporadic E layers. In *Aeronomy of the Earth's atmosphere-ionosphere, IAGA book Series* (Vol. 29, pp. 381–394). Dordrecht, Netherlands: Springer. https://doi.org/10.1007/978-94-007-0326-1_29

Haldoupis, C., Meek, C., Christakis, N., Pancheva, D., & Bourdillon, A. (2006). Ionogram height-time intensity observations of descending sporadic E layers at mid-latitude. *Journal of Atmospheric and Solar - Terrestrial Physics*, *68*(3-5), 539–557. https://doi.org/10.1016/j.jastp.2005.03.020

Harper, R. M. (1977). Tidal winds in the 100- to 200-km region at Arecibo. *Journal of Geophysical Research*, *82*(22), 3243–3250. https://doi.org/10.1029/JA082i022p03243

Hook, W. H. (1970). Ionospheric response to internal gravity waves 2. Lower F region response. *Journal of Geophysical Research*, *75*(34), 7229–7238. https://doi.org/10.1029/JA075i034p07229

Kikuchi, T., Lühr, H., Schlegel, K., Tachihara, H., Shinohara, M., & Kitamura, T.-I. (2000). Penetration of auroral electric fields to the equator during a substorm. *Journal of Geophysical Research*, *105*(A10), 23,251–23,261. https://doi.org/10.1029/2000JA900016

Knecht, R. W., & McDuffie, R. E. (1962). On the width of the equatorial Es belt. In E. K. Smith & S. Matsushita (Eds.), *Ionospheric sporadic E*, (pp. 215–218). New York: Pergamon Press. https://doi.org/10.1016/B978-0-08-009744-2.50022-9

Lanchester, B. S., Nygren, T., Huskomen, A., Turnen, T., & Jarvis, M. J. (1991). Sporadic-E as trace of atmospheric gravity waves. *Planetary and Space Science*, *39*(10), 1421–1434. https://doi.org/10.1016/0032-0633(91)90021-2

Li, G., Ning, B., Zhao, B., Liu, L., Wan, W., Ding, F., … Yumoto, K. (2009). Characterizing the 10 November 2004 storm-time middle-latitude plasma bubble event in Southeast Asia using multi-instrument observations. *Journal of Geophysical Research*, *114*, A07304. https://doi.org/10.1029/2009JA014057

Maruyama, T. (2006). Extreme enhancement in total electron content after sunset on 8 November 2004 and its connection with storm enhanced density. *Geophysical Research Letters*, *33*, L20111. https://doi.org/10.1029/2006GL027367

Maruyama, N., Richmond, A. D., Fuller-Rowell, T. F., Codrescu, M. V., Sazykin, S., Tof-foletto, F. R., … Millward, G. H. (2005). Interaction between direct penetration and disturbance dynamo electric fields in the storm-time equatorial ionosphere. *Geophysical Research Letters*, *32*, L17105. https://doi.org/10.1029/2005GL023763

Mathews, J. D., & Bekeny, F. S. (1979). Upper atmosphere tides and the vertical motion of ionospheric sporadic layers at Arecibo. *Journal of Geophysical Research*, *84*(A6), 2743–2750. https://doi.org/10.1029/JA084iA06p02743

Moro, J., Denardini, C. M., Resende, L. C. A., Chen, S. S., & Schuch, N. J. (2016a). Equatorial E region electric fields at the dip equator: 1. Variabilities in eastern Brazil and Peru. *Journal of Geophysical Research: Space Physics*, *121*, 10,220–10,230. https://doi.org/10.1002/2016JA022751

Moro, J., Denardini, C. M., Resende, L. C. A., Chen, S. S., & Schuch, N. J. (2016b). Equatorial E region electric fields at the dip equator: 2. Seasonal variabilities and effects over Brazil due to the secular variation of the magnetic equator. *Journal of Geophysical Research: Space Physics*, *121*, 10,231–10,240. https://doi.org/10.1002/2016JA022753

Moro, J. M., Denardini, C. M., Resende, L. C. A., Chen, S. S., & Schuch, N. J. (2016c). Influence of uncertainties of the empirical models for inferring the E-region electric fields at the dip equator. *Earth, Planets and Space*, *68*(1), 103. https://doi.org/10.1186/s40623-016-0479-0

Piggot, W., & Rawer, K. (1972). Handbook of ionogram interpretation and reduction, Edited by U.S. Department of Commerce, 352.

Rastogi, R. G., Chandra, H., Condori, L., Abdu, M. A., Reinisch, B., Tsunoda, R. T., … Maruyama, T. (2012). Abnormally large magnetospheric electric field on 9 November 2004 and its effect on equatorial ionosphere around the world. *Journal of Earth System Science (Indian Academy of Sciences)*, *121*(5), 1145–1161. https://doi.org/10.1007/s12040-012-0231-5

Resende, L. C. A., Batista, I. S., Denardini, C. M., Batista, P. P., Carrasco, J. A., Andrioli, V. F., & Moro, J. (2017). Simulations of blanketing sporadic E-layer over the Brazilian sector driven by tidal winds. *Journal of Atmospheric and Solar - Terrestrial Physics*, *154*, 104–114. https://doi.org/10.1016/j.jastp.2016.12.012

Resende, L. C. A., Batista, I. S., Denardini, C. M., Batista, P. P., Carrasco, J. A., Andrioli, V. F., … Chen, S. S. (2016). Competition between winds and electric fields in the formation of blanketing sporadic E layers at equatorial regions. *Earth, Planets and Space*, *68*(1), 201. https://doi.org/10.1186/s40623-016-0577-z

Resende, L. C. A., Denardini, C. M., & Batista, I. S. (2013). Abnormal f_bE_s enhancements in equatorial Es layers during magnetic storms of solar cycle 23. *Journal of Atmospheric and Solar - Terrestrial Physics*, *102*, 228–234. https://doi.org/10.1016/j.jastp.2013.05.020

Richmond, A. D., Peymirat, C., & Roble, R. G. (2003). Long-lasting disturbances in the equatorial ionospheric electric field simulated with a coupled magnetosphere-ionosphere-thermosphere model. *Journal of Geophysical Research*, *108*(A3), 1118. https://doi.org/10.1029/2002JA009758

Scherliess, L., Schunk, R. W., Sojka, J. J., Thompson, D. C., & Zhu, L. (2006). Utah State University global assimilation of Ionospheric measurements Gauss-Markov Kalman filter model of the ionosphere: Model description and validation. *Journal of Geophysical Research*, *111*, A11315. https://doi.org/10.1029/2006JA011712

Tsunoda, R. T. (2008). On blanketing sporadic E and polarization effects near the equatorial electrojet. *Journal of Geophysical Research*, *113*, A09304. https://doi.org/10.1029/2008JA01315

Vijaya Lekshmi, D., Balan, N., Vaidyan, V. K., Alleyne, H., & Bailey, G. J. (2008). Response of the ionosphere to super geomagnetic storms: Observations and modeling. *Advances in Space Research*, *41*(4), 548–555. https://doi.org/10.1016/j.asr.2007.08.029

Whitehead, J. D. (1989). Recent work on mid-latitude and equatorial sporadic-E. *Journal of Atmospheric and Terrestrial Physics*, *51*(5), 401–424. https://doi.org/10.1016/0021-9169(89)90122-0, Retrieved from http://www.sciencedirect.com/science/article/pii/0021916989901220